ELSEVIER

Engineering Analysis with Boundary Elements 27 (2003) 853–862

ENGINEERING ANALYSIS *with* BOUNDARY ELEMENTS

www.elsevier.com/locate/enganabound

A radial boundary node method for two-dimensional elastic analysis

Hua Xie[a], Toyoaki Nogami[a], Jianguo Wang[b,*]

[a]*Department of Civil Engineering, The National University of Singapore, Singapore, Singapore 119260*
[b]*Tropical Marine Science Institute, The National University of Singapore, Singapore, Singapore 119260*

Received 7 September 2001; revised 3 September 2002; accepted 23 January 2003

Abstract

The boundary node method (BNM) takes the advantages of both the boundary integral equation in dimension reduction and the moving least-square (MLS) approximation in elements elimination. However, the BNM inherits the deficiency of the MLS approximation, in which the shape functions lack the delta function property. As a result boundary conditions could not be exactly implemented for the BNM. In this paper, a radial boundary node method (RBNM) is proposed. The RBNM uses radial basis functions (RBFs) instead of the MLS to construct its interpolation. Consequently, the interpolation function could pass through nodes exactly, and the shape functions are of the delta function property. The exponential (EXP) and the multiquadric (MQ) RBFs are used in the current RBNM, and their shape parameters are studied in detail through some analyses of two-dimensional elastic problems. The suitable ranges of the shape parameters are proposed for both the EXP and the MQ basis functions. It is found that the RBNM is as accurate as or even more precise than the BEM. This suggests that the current RBNM could be robust and applicable.

Keywords: Boundary integral equation; Boundary node method; Point interpolation method; Radial basis function; Shape parameter

1. Introduction

Partial differential equations are usually the mathematical expressions of physical problems. Analytical solutions are always the first choice, but only a handful of simple problems can be solved analytically. In most cases, numerical methods are used to obtain approximate solutions. The finite element method (FEM) [1] as a popular tool has been well developed in the past years. However, the FEM is still cumbersome for problems with large domains, for which cases descretizing process is time consuming. To overcome this difficulty associated with the FEM, the boundary element method (BEM) [2] appears to be an attractive alternative. In the BEM, only the boundary of the domain needs to be discretized. This reduces the problem dimension by one and thus largely reduces the time in meshing. The BEM still uses elements to implement both interpolation and integration. In case of large deformation or moving boundary problems, the elements may be heavily distorted, and thus the shape functions based on elements could be of poor properties. This may cause the BEM results unacceptable.

Over the past years, the element-free methods [3] have been developed to overcome the difficulties associated with 'elements'. Most element-free methods are based on the moving least-square (MLS) [4] approximation and developed to solve domain problems. A boundary node method (BNM) [5] combines the MLS with the boundary integral equation (BIE) to deal with boundary-value problems [6]. The BNM is different from the BEM in nodal interpolation. In the BNM, the nodes for interpolation are not bounded by the integral element, while in the BEM the nodes for interpolation completely coincide with the integral element. The BNM not only inherits the advantage of the dimension reduction, but also extends its capability to deal with complicated boundaries such as moving boundaries. However, the BNM cannot exactly satisfy boundary conditions, since its shape functions constructed by the MLS approximation lack the delta function property. Ref. [7] partly solved this problem by introducing special strategy. A radial point interpolation method (radial PIM) [8] was proposed to construct the shape functions. The radial PIM has been successfully applied to some domain problems in solid [8,9] and in Biot's consolidation problems [10,11]. The shape functions derived by the radial PIM acquire the delta function property, and thus the boundary conditions could be easily

* Corresponding author.
E-mail address: tmswjg@nus.edu.sg (J.G. Wang).

0955-7997/03/$ - see front matter © 2003 Published by Elsevier Ltd.
doi:10.1016/S0955-7997(03)00027-4

and exactly satisfied. Furthermore, in the radial PIM the Cartesian co-ordinates can be directly applied to arbitrarily distributed nodes. In the BNM a curvilinear co-ordinates must be used, otherwise the singularity of the moment matrix may occur whenever the boundary nodes lie on a straight line [5]. The Cartesian co-ordinates are more straightforward than the curvilinear co-ordinates, and thus the formulations constructed by the radial PIM are more feasible.

Two kinds of radial basis functions (RBFs), the multi-quadric (MQ) and the exponential (EXP) radial basis functions [8], were used to construct the shape functions in the radial PIM. The shape parameters involved in these two basis functions were studied for domain problems [9]. Although the radial PIM has been extended to the BPIM [12], the shape parameters have not been studied till now. Previous works [9,13–15] have indicated that the optimal shape parameters depend on both interpolation and weak forms of governing equations. Therefore, it is necessary to explore the suitable ranges of the shape parameters for the BIE weak form.

The RBF was first used to solve partial differential equations in the early 1990s. Kansa [16] was the pioneer who adopted the MQ basis function to solve the Navier–Stokes equation in fluid mechanics. His method was similar to the finite difference method, but it is less sensitive to nodal distribution. Collocation methods utilizing the RBFs have been developed recently as promising element-free methods [17–20], but they have three demerits. The first lies in their treatment of internal and external boundary conditions. The current methods are almost the same as the finite difference method, and thus they may lose some properties of the system stiffness matrix such as symmetry. The second demerit is that higher derivatives of shape functions are required in computation. This is sometimes difficult in practice. Mesh-less methods based on the weak form, such as the radial PIM, eliminate the above disadvantages [8]. The weak form requires lower order of derivatives in internal points and along boundaries. Finally, all the collocation methods are developed to solve domain problems. In case of large domains, their computation efficiencies may be very low. A BNM with dimension reduction could be more promising.

A new numerical method, the radial boundary node method (RBNM), is proposed in this paper. The RBNM is formulated for two-dimensional (2D) elastic problems. It combines the BIE and the RBFs to decrease the problem dimension by one. This dimension reduction is useful for infinite/semi-infinite domains problems. Furthermore, the RBFs bring the following three merits to the current RBNM: (1) interpolation is implemented by a cluster of nodes in stead of elements, and thus tracing the large strain boundary becomes easier; (2) the interpolation satisfies the delta function property, so implementing boundary conditions in the RBNM is much easier than that in the BNM; and 3) the potential matrix singularities associated with use of only polynomial basis [11] is avoided. The shape parameters are studied in detail for the MQ and the EXP radial basis functions. The ranges of the shape parameters suitable for the current RBNM are found out. This is necessary to make the current RBNM robust and applicable to real problems.

This paper is organized as follows: Section 2 presents the boundary integral equation; Section 3 introduces numerical implementation with the radial point interpolation; Section 4 studies the influences of shape parameters on the accuracy of the RBNM and recommends the suitable ranges of the shape parameters; and Section 5 presents the conclusion.

2. Boundary integral equation for 2D elasticity

For a 2D solid mechanics problem, the equilibrium equation and the boundary conditions are

$$\sigma_{kj,j} + b_k = 0 \qquad \text{in } \Omega \tag{1}$$

$$u_k = \bar{u}_k \qquad \text{on } \Gamma_1 \tag{2}$$

$$p_k = \sigma_{kj} n_j = \bar{p}_k \qquad \text{on } \Gamma_2$$

where $j, k = 1, 2$; σ_{kj} is the stress tensor; b_k is the component of body forces; $\bar{u}_k$ and $\bar{p}_k$ are the prescribed displacement and traction; and n_j is the outward normal vector. The whole boundary $\Gamma = \Gamma_1 \cup \Gamma_2$.

Eq. (1) can be expressed as a boundary integral form [2]

$$c_{lk}(\xi)u_k(\xi) + \int_\Gamma p^*_{lk}(X-\xi)u_k(X)\mathrm{d}\Gamma = \int_\Gamma u^*_{lk}(X-\xi)p_k(X)\mathrm{d}\Gamma \tag{3}$$

where ξ denotes the position on the boundary where a unit force is located; X denotes the location of any field point; u^*_{lk} and p^*_{lk} are the fundamental solutions which represent the kth components of displacements and tractions due to a unit point load in the l-direction; and $c_{lk}(\xi)$ is a coefficient related to the boundary smoothness.

3. Numerical implementation by the RBNM

3.1. Spatial discretization and boundary

The unknowns in Eq. (3) are the boundary displacement u_k and the traction p_k. The boundary Γ is divided into NE cells for integration, and in each cell, the integration can be implemented by Gaussian quadrature. Approximations at each Gaussian point can be expressed as

$$u_k = \sum_{x=1}^{\mathrm{ND}} \phi_{kx} u_x, \qquad p_k = \sum_{x=1}^{\mathrm{ND}} \phi_{kx} p_x \tag{4}$$

where ND is the number of nodes in the influence domain. If Eq. (4) is introduced into Eq. (3), a discrete system equation

can be obtained as

$$c_{lk}^{i}u_{k}^{i}+\sum_{j=1}^{\mathrm{NE}}\sum_{m=1}^{\mathrm{NG}}\sum_{x=1}^{\mathrm{ND}}W_{m}(p_{lk}^{*}\phi_{kx}J)_{m}u_{x}$$

$$=\sum_{j=1}^{\mathrm{NE}}\sum_{m=1}^{\mathrm{NG}}\sum_{x=1}^{\mathrm{ND}}W_{m}(u_{lk}^{*}\phi_{kx}J)_{m}p_{x} \tag{5}$$

where NG is the total number of Gauss points in a quadrature cell; W_m is the weight of Gaussian quadrature including the area at mth Gaussian point; J is the Jacobian matrix; u_x and p_x are the nodal values at xth node; and ϕ_{kx} is the shape function of x node to Gaussian point k.

Eq. (5) can be expressed in matrix form as follows:

$$\mathbf{Hu}=\mathbf{Gp} \tag{6}$$

where **H** and **G** are the assembled matrices with coefficients determined from Eq. (5); and **u** and **p** are the global nodal displacement and traction vectors, respectively, which satisfy the boundary conditions as shown in Eq. (2).

Taking all unknowns to the left side, Eq. (6) can be rewritten into the following form:

$$\mathbf{Ax}=\mathbf{F} \tag{7}$$

where **x** is the unknown; **A** is the system stiffness matrix; and **F** is the known vector determined by the known boundary conditions. The shape functions in Eq. (4) for interpolation will be determined by a radial boundary node interpolation as below.

3.2. Radial boundary node interpolation

In an influence domain with ND scattered nodes, the displacement **u** can be approximated as

$$\mathbf{u}(X)=\mathbf{B}^{\mathrm{T}}(X)\mathbf{a} \tag{8}$$

where $B_i(X)$ is a RBF and a_i is a coefficient. They are expressed in vectors as

$$\mathbf{B}^{\mathrm{T}}(X)=[B_1(X),B_2(X),\ldots,B_{\mathrm{ND}}(X)] \tag{9}$$

$$\mathbf{a}^{\mathrm{T}}=[a_1,a_2,\ldots,a_{\mathrm{ND}}]$$

Let the approximation expressed by Eq. (8) pass through all the ND scattered nodes, that is

$$\hat{\mathbf{u}}=\mathbf{B}_0\mathbf{a} \tag{10}$$

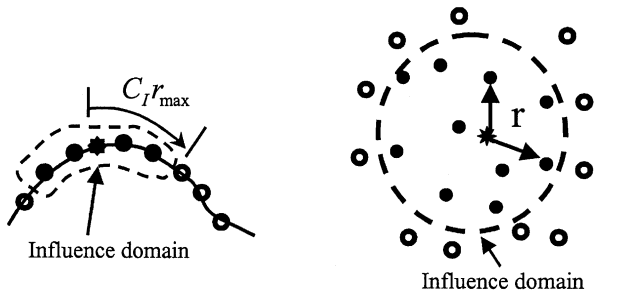

(a) Node selection for RBNM (b) Node selection for radial PIM

Fig. 1. Comparison of node selection procedure for the RBNM and the radial PIM.

where

$$\hat{\mathbf{u}}=[u_1,u_2,\ldots,u_{\mathrm{ND}}]^{\mathrm{T}} \tag{11}$$

$$\mathbf{B}_0=\begin{bmatrix} B_1(x_1,y_1) & B_2(x_1,y_1) & \cdots & B_{\mathrm{ND}}(x_1,y_1) \\ B_1(x_2,y_2) & B_2(x_2,y_2) & \cdots & B_{\mathrm{ND}}(x_2,y_2) \\ \vdots & \vdots & \ddots & \vdots \\ B_1(x_{\mathrm{ND}},y_{\mathrm{ND}}) & B_2(x_{\mathrm{ND}},y_{\mathrm{ND}}) & \cdots & B_{\mathrm{ND}}(x_{\mathrm{ND}},y_{\mathrm{ND}}) \end{bmatrix} \tag{12}$$

Thus, **a** can be obtained as

$$\mathbf{a}=\mathbf{B}_0^{-1}\hat{\mathbf{u}} \tag{13}$$

and the displacement is expressed as

$$\mathbf{u}(X)=\Phi(X)\hat{\mathbf{u}} \tag{14}$$

where the shape function vector is

$$\Phi(X)=\mathbf{B}^{\mathrm{T}}(X)\mathbf{B}_0^{-1}$$

$$=[\phi_1(X),\phi_2(X),\ldots,\phi_k(X),\ldots,\phi_{\mathrm{ND}}(X)] \tag{15}$$

and its component is

$$\phi_k(X)=\sum_{i=1}^{\mathrm{ND}}B_i(X)\bar{B}_{i,k} \tag{16}$$

where $\bar{B}_{i,k}$ is the element of matrix $\mathbf{B}_0^{-1}$.

It is noted that the displacement and the traction are discretized using the same shape functions as given in Eq. (4). Although Eq. (14) has the same form as that based on the radial PIM [9], their influence domains are different. The RBNM has an influence domain only along boundary, while the radial PIM has an influence domain within problem

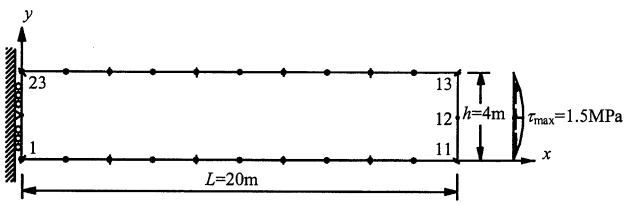

Fig. 2. Cantilever beam subjected to end loading.

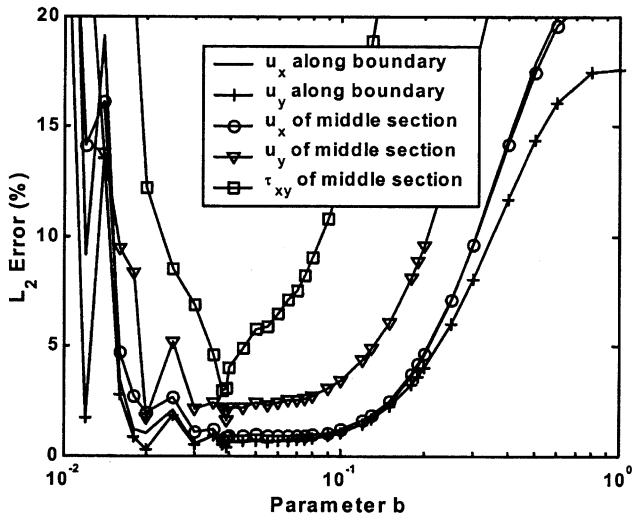

(a) 24 Nodes

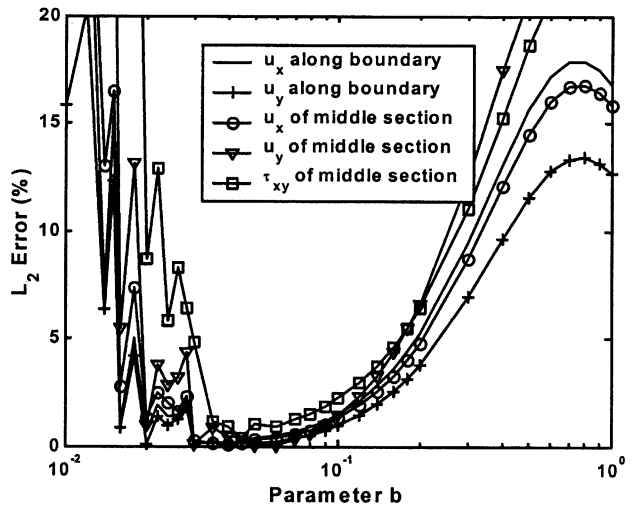

(b) 48 Nodes

Fig. 3. L_2-error with different b for the EXP RBF.

domain. Fig. 1 shows the difference between the two methods.

Two particular forms of RBFs [8] will be studied in this paper. One is the EXP RBF [21], and the other is the MQ RBF [22]. The EXP RBF has the following form

$$B_i(x,y) = \exp\left(-b\left(\frac{r_i}{r_{\max}}\right)^2\right) \tag{17}$$

where b is a shape parameter.

The MQ RBF has the following form

$$B_i(x,y) = \left(\left(\frac{r_i}{r_{\max}}\right)^2 + R\right)^q \tag{18}$$

where q and R are shape parameters, and $r_{\max}$ is the maximum distance of neighborhood node within an influence domain. It is noted that the R instead of R^2 [8] is used.

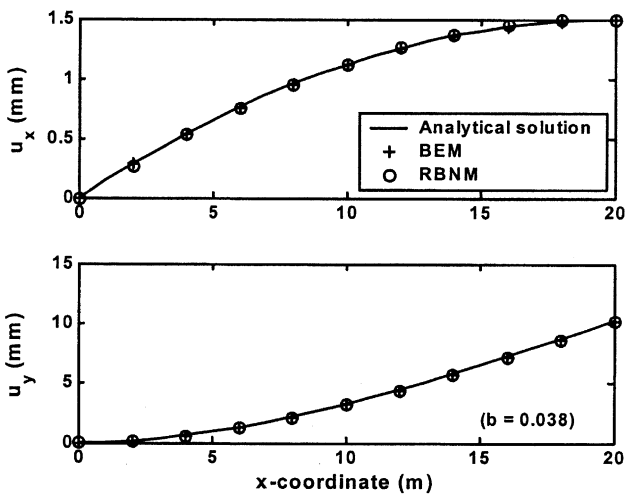

Fig. 4. Displacements along the lower boundary (EXP basis).

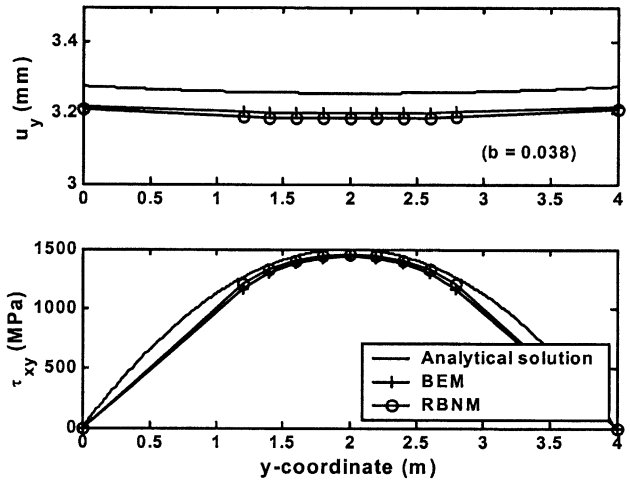

Fig. 5. Displacement and shear stress along the middle section (EXP basis).

4. Shape parameters in the RBNM and applications

This section will study the shape parameters through cantilever beam problem and apply these shape parameters to other problems. In the radial PIM, Wang and Liu [8,9] proposed the suitable shape parameter as $b = 0.002–0.03$ for the EXP RBF and $q = 0.98–1.03$ for the MQ RBFs. However, whether these shape parameters are applicable to the RBNM or not has not been examined yet. In this paper, normalized EXP and MQ RBFs are used, so how the shape parameters are different from that in the radial PIM should be studied.

4.1. Cantilever beam under end loading and error criterion

A cantilever beam as shown in Fig. 2 is studied as an example. The plane stress condition is assumed. The elastic constants are the shear modulus $G = 8000$ MPa and the Poisson ratio $\nu = 0.20$. The Young's modulus can be

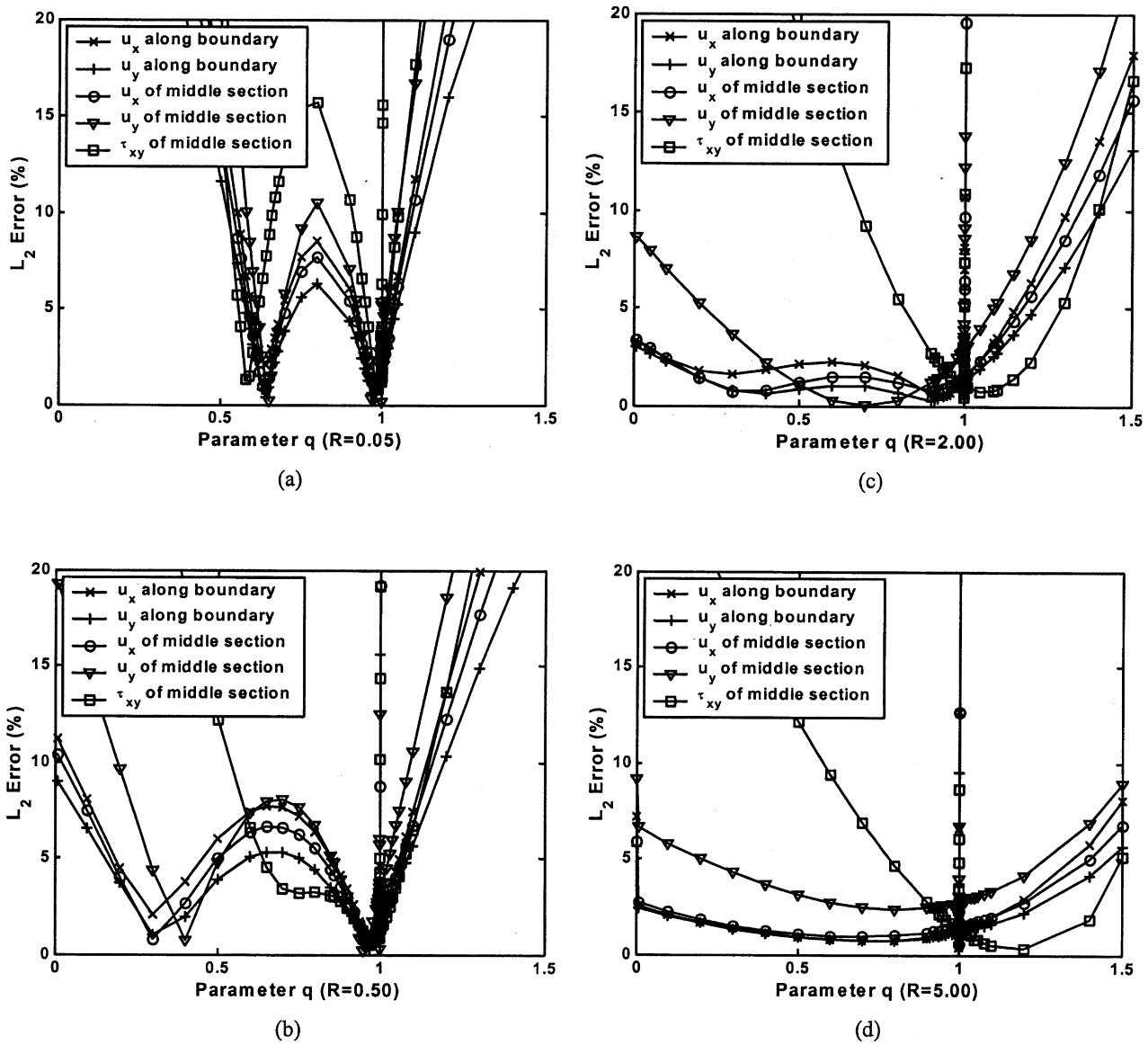

Fig. 6. L_2-error with different R and q for the MQ RBF.

computed from $E = 2(1 + \nu)G$. A total loading P (= 4000 kN) is applied at the free end in such a way that the shear stress has a parabolic distribution with the maximum value of $\tau_{max} = 1.5$MPa. Analytical solutions can be found for this problem [23],

$$u_x = -\frac{P(y-h/2)}{6EI}\left\{(6L-3x)x+(2+\nu)\left[\left(y-\frac{h}{2}\right)^2-\frac{h^2}{4}\right]\right\}$$

$$u_y = \frac{P(y-h/2)}{6EI}\left[3\nu\left(y-\frac{h}{2}\right)^2(L-x)+(4+5\nu)\frac{h^2x}{4}+(3L-x)x^2\right] \quad (19)$$

$$\sigma_x(x,y) = -\frac{P(L-x)(y-h/2)}{I}$$

$$\sigma_y(x,y) = 0 \quad (20)$$

$$\sigma_{xy}(x,y) = \frac{P}{2I}\left[\frac{h^2}{4}-\left(y-\frac{h}{2}\right)^2\right]$$

where $I = h^3/12$.

An L_2 error norm is defined to evaluate the RBNM performance:

$$\varepsilon = \frac{1}{|f|_{max}}\sqrt{\frac{1}{N}\sum_{i=1}^{N}(f^n - f^e)^2} \times 100\ (\%) \quad (21)$$

where ε is the percentage L_2 error over N nodes; f^n and f^e refer to the nodal values obtained by the numerical method and exact solutions, respectively; $|f|_{max}$ is the maximum value of f over N nodes. Here f may be a component of displacements or tractions. The radius of the influence domain is 2.5 times of r_{max}($C_I = 2.5$). This can encompass 3–7 nodes in each influence domain. A corner node is regarded as the end point of a boundary.

4.1.1. Shape parameter b for the EXP radial basis function

Fig. 3 shows the L_2 errors for the displacements and the shear stress along the middle section and the lower boundary. Fig. 3(a) is the case with 24 nodes and Fig. 3(b)

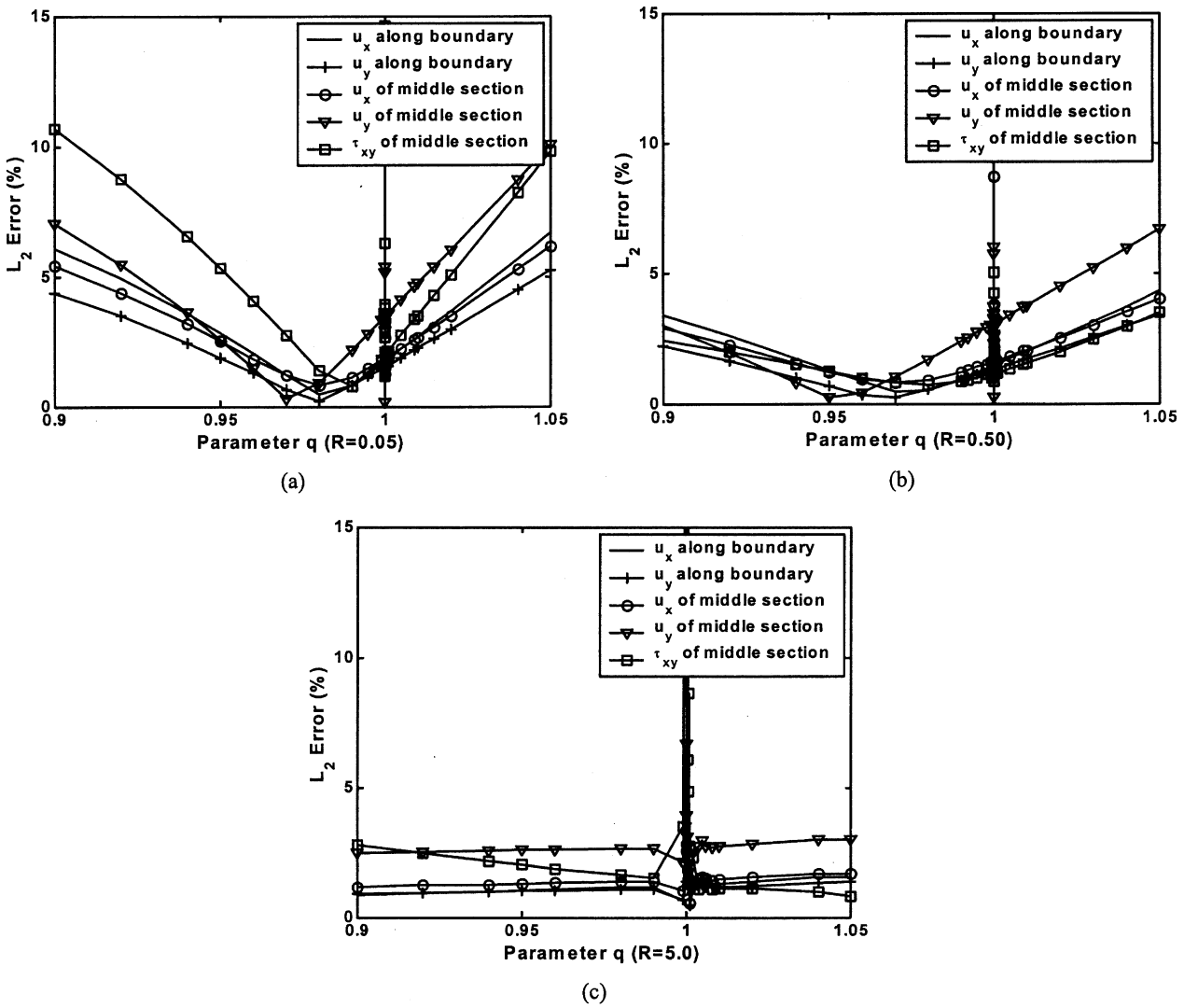

Fig. 7. L_2-error for q varying from 0.9 to 1.05.

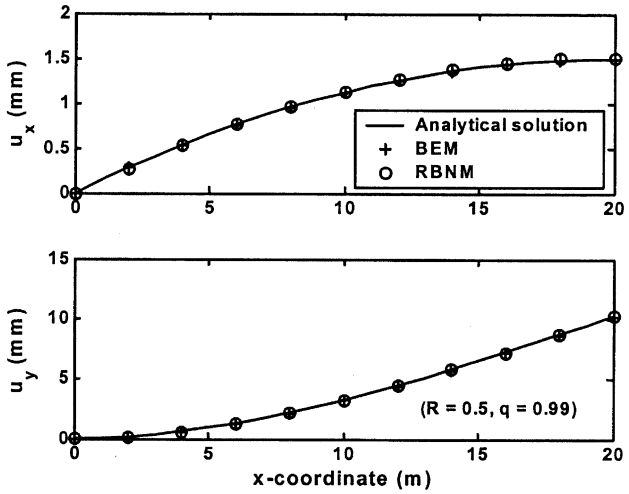

Fig. 8. Displacements of the lower boundary with the MQ basis.

is the case with 48 nodes. The curves for both cases have the similar patterns although the error is lower for the 48-node case. It is true that the loading distribution at the end of the beam can be described more accurately by using more nodes. It is also observed that the L_2 error fluctuates when $b < 0.03$ and becomes stable when $0.03 \leq b \leq 0.1$. This range of shape parameters is different from that shown in the radial PIM [8,9]. Possible reasons for this difference may be due to the interpolation implemented only along the boundary and the use of the weak form of BIE in the current RBNM. Fig. 4 compares the displacements along the lower boundary and Fig. 5 compares the displacement and shear stress along the middle section. The results obtained by the BEM [2] and the analytical solution are also plotted for comparison. The numerical results obtained for the 24-node case when the shape parameter $b = 0.038$ for the EXP RBF. The results show that the current RBNM produces results in good agreement with the analytical solutions. Furthermore, shape parameter b that ranged from 0.03 to 0.1 could produce steady results and small errors as well.

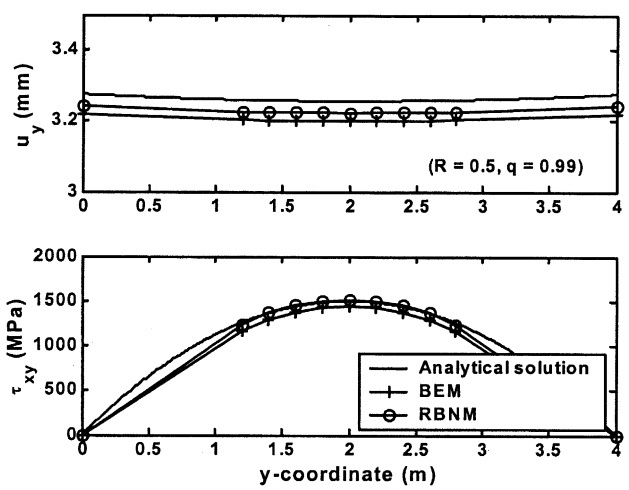

Fig. 9. Displacement and shear stress along the middle section with the MQ basis.

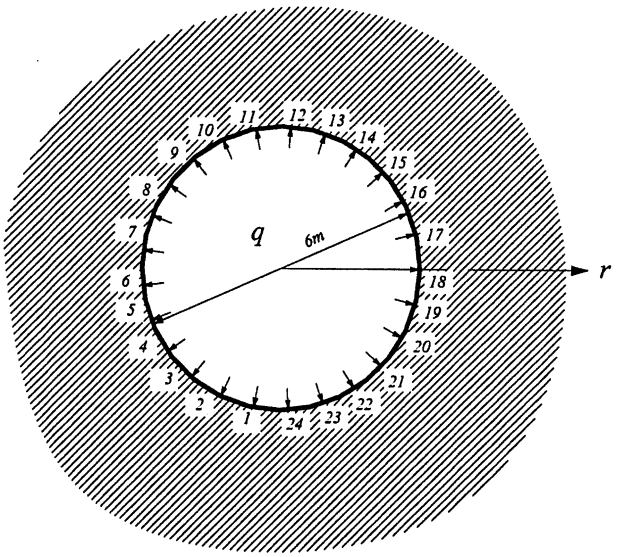

Fig. 10. Circular cavity under internal pressure.

4.1.2. Shape parameters R and q for the MQ radial basis function

Fig. 6(a)–(d) show the L_2 errors computed with varying shape parameters R and q for 24-node case. Similar results can be obtained for the 48-node case so they are not shown here. Fig. 7(a)–(c) shows the L_2 errors due to the fine tuning of the shape parameter q around 1. Generally there are two obvious regions where the L_2 errors approach to zero. One is in the immediate vicinity of $q = 1$, and it does not change with different values of R. The other is located at some place where $0 < q < 1$ and moves with varying values of R. When R increases, the second region approaches to origin and finally vanishes when $R \geq 2.0$. This observation is different from that obtained by the radial PIM in which only the first region was observed [9]. When $q = 1$, the L_2 errors become very large. This may be due to the singularity of the matrix $\mathbf{B}_0$ at $q = 1$.

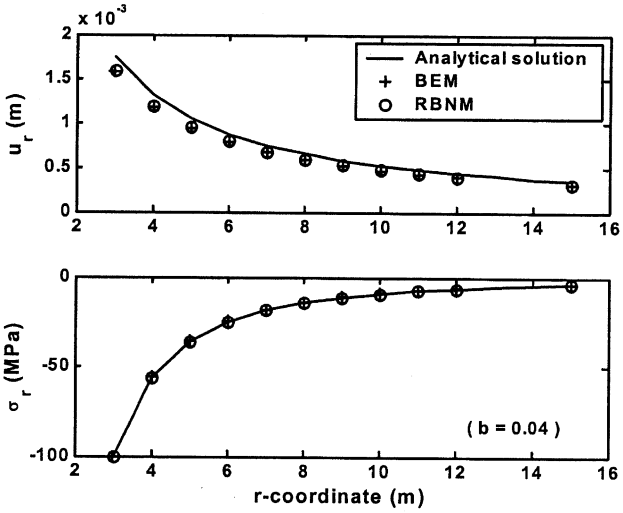

Fig. 11. Displacement and stresses of the interior section along r-coordinate.

The above figures show that errors are small when the shape parameter q ranges from 0.96 to 0.99 or from 1.01 to 1.05. Although errors near $q = 1$ are small for any value of R, smaller R is still suggested since $\mathbf{B}_0$ has a smaller matrix condition number for smaller R.

The results computed by the BNM are compared with those computed by the BEM and the analytical solutions in Figs. 8 and 9. The shape parameters for the MQ RBF are taken as $R = 0.5$ and $q = 0.99$. Compared with the BEM, the current RNBM produces results in better agreement with analytical solutions for both displacements and stresses.

4.2. Circular cavity in an infinite medium under internal pressure

This example demonstrates the applicability of the shape parameters that are obtained from the cantilever beam problem. Fig. 10 describes a circular cavity in an infinite medium subjected to an internal pressure. This is a curved boundary problem. The internal boundary is discretized with 24 nodes, and node 18 is completely fixed to prevent from rigid body displacements. The shape parameter $b = 0.04$ is used for the EXP basis function. Fig. 11 shows the comparisons of displacements and stresses computed by the RBNM, the BEM and the analytical solutions. They are in good agreement. Fig. 12(a)–(d) studies the shape parameters R and q for the MQ basis function. These curves have similar patterns to those of cantilever beam problem as shown in Fig. 6. The shape parameters obtained from the cantilever beam problem can be also used for the cavity problem.

4.3. Half-space problem under stripe loading

This example will use the shape parameters obtained from the cantilever beam problem. A plane strain half-space

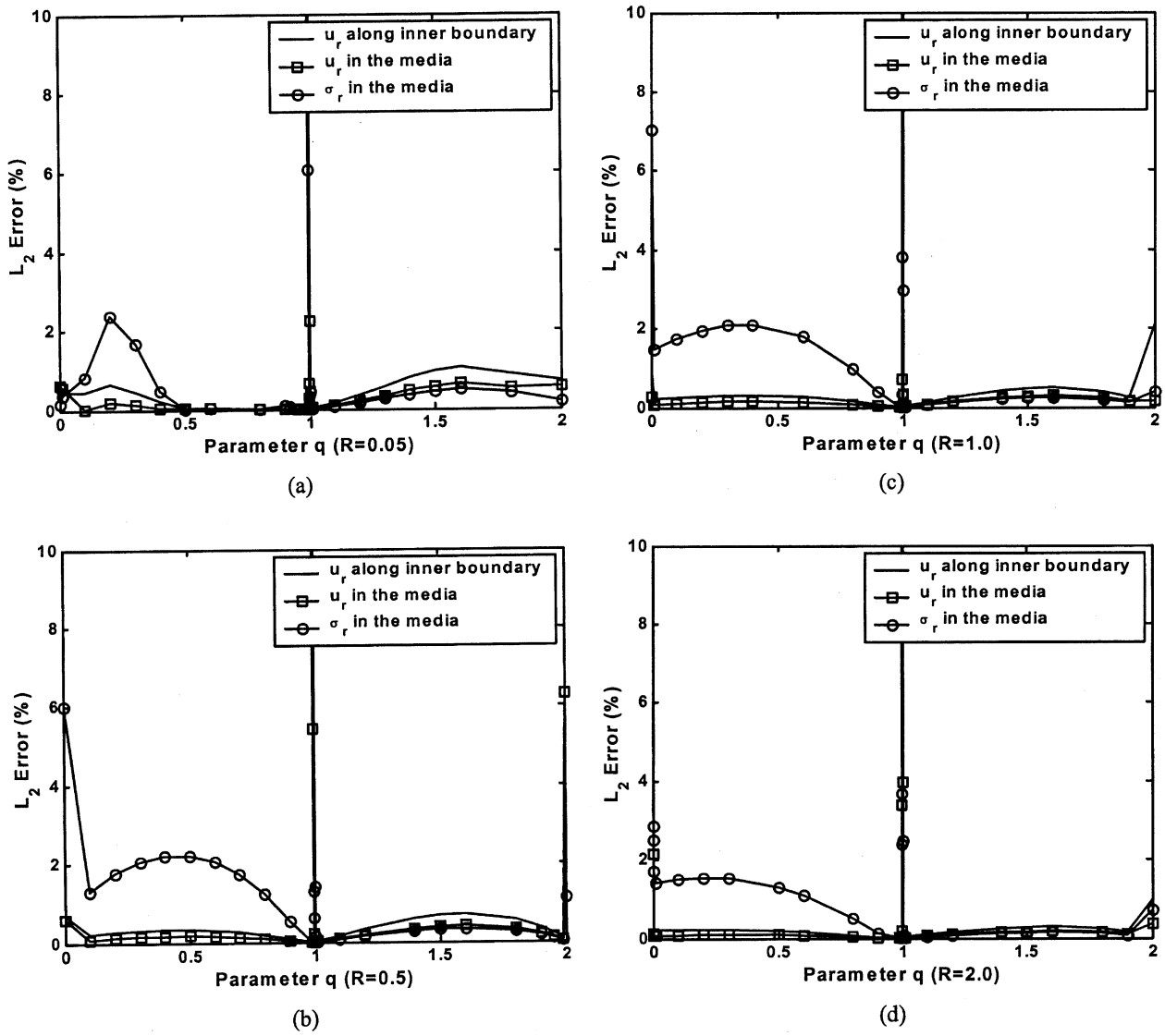

Fig. 12. L_2-error with different R and q for the MQ RBF.

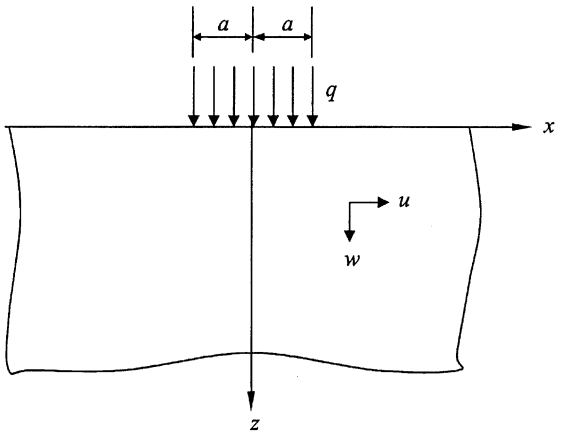

(a) Elastic half-plane subjected to a uniform loading q of width $2a$

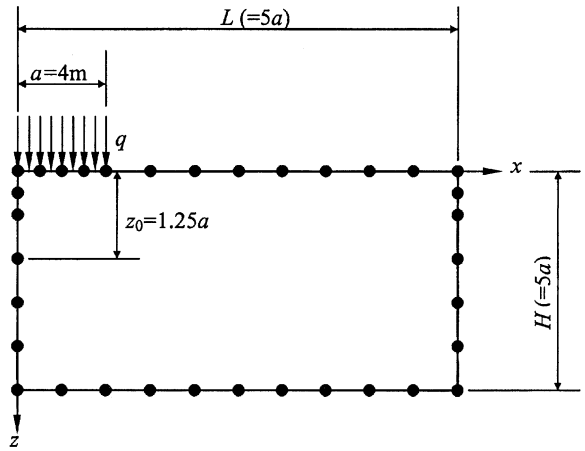

(b) Meshless model for half-plane problem

Fig. 13. Nodal model for half-plane problem.

problem as shown in Fig. 13(a) is studied. For convenience, a bounded domain is considered to develop its numerical model, and some specified point is treated as the reference. Fig. 13(b) shows the arrangement of nodes. The shape parameters for the MQ basis function are taken as $R = 0.5$ and $q = 0.99$. Fig. 14(a) and (b) shows the comparison of the displacement and the stresses, respectively. The displacement u_z is along the upper boundary. The distributions of the stresses are along a horizontal plane located at $z = z_0$. The results computed by the RBNM are very close to the analytical solutions and, in some cases, are even better than those computed by the BEM. This further indicates the excellent capability of the current RBNM.

5. Conclusions

This paper presents a new boundary node method—the RBNM for the 2D elastic problems. The RBNM is formulated by combining the redial PIM with the BIE. Two RBFs, the MQ and the EXP basis functions, are incorporated into the RBNM. The shape parameters are

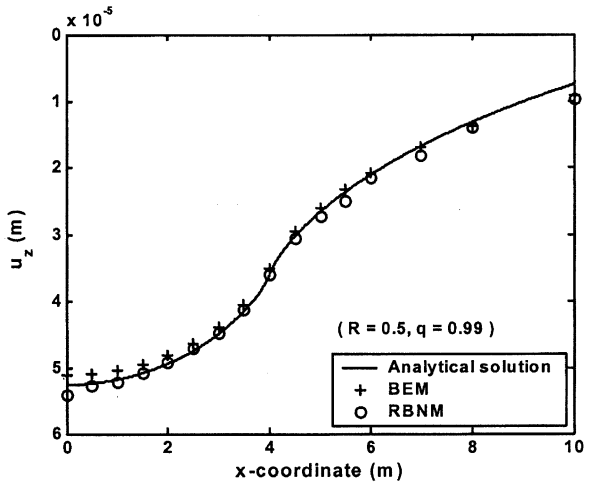

(a) Displacement in z direction along the upper boundary

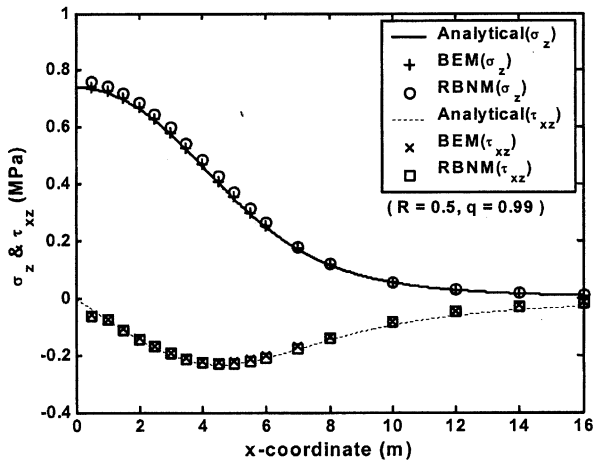

(b) Distribution of stresses along a horizontal plane where $z = z_0$

Fig. 14. Distribution of displacement and stresses.

studied in detail for a cantilever beam problem and a cavity problem. The shape parameters are also applied to the cavity problem for the EXP basis function and a half-space problem for the MQ basis function. The following conclusions can be drawn from these studies:

First, the RBNM can get as accurate results as the BEM and sometimes the RBNM can get even higher accuracy than the BEM. This is due to its higher accuracy of interpolation. The RBNM uses a cluster of nodes instead of elements to construct its interpolation. This makes the node more easily add or remove. Therefore, the RBNM is more effective than the BEM for solving problems with moving boundaries.

Second, suitable ranges of shape parameters are obtained in this study. Numerical examples indicate that the suitable ranges of shape parameter $b = 0.03–0.1$ for the EXP basis function and $q = 0.96–0.99$ or $1.01–1.05$ regardless of shape parameter R for the MQ basis function. In addition, the accuracy is generally acceptable as long as shape

parameter R ranges from 0.05 to 2.0. Above shape parameters are suitable not only for cantilever beam problem, but also for cavity and half-space problems.

Third, in use of the MQ basis function, errors would reach their lowest in two regions. The first one is near $q = 1$ regardless of the value of R. The second region of q where the errors would reach their minimums is sensitive to shape parameter R. When R is small, the second region would approach to the origin as R increases. When $R \geq 2.0$, the second region would vanish. This phenomenon was not observed in the radial PIM.

References

[1] Zienkiewicz OC. Finite element method. London: McGraw-Hill; 1977.
[2] Brebbia CA, Dominguez J. Boundary elements—an introductory course, 2nd ed. New York: McGraw-Hill; 1992. p. 262–5.
[3] Belytschko T, Krongauz Y, Organ D, Fleming M, Krysl P. Meshless methods: an overview and recent developments. Comput Meth Appl Mech Engng 1996;139:3–47.
[4] Lancaster P, Salkauskas K. Surfaces generated by moving least squares methods. Math Comput 1981;37:141–58.
[5] Mukherjee YX, Mukherjee S. The boundary node method for potential problems. Int J Numer Meth Engng 1997;40(5): 797–815.
[6] Chati MK, Mukherjee S, Mukherjee YX. The boundary node method for three-dimensional linear elasticity. Int J Numer Meth Engng 1999; 46(8):1163–84.
[7] Mukherjee YX, Mukherjee S. On boundary conditions in the element-free Galerkin method. Comput Mech 1997;19(4):264–70.
[8] Wang JG, Liu GR. A point interpolation meshless method based on radial basis functions. Int J Numer Meth Engng 2002;54(11): 1623–48.
[9] Wang JG, Liu GR. On the optimal shape parameters of radial basis functions used for 2-D meshless methods. Comput Meth Appl Mech Engng 2002;191:2611–30.
[10] Wang JG, Liu GR, Lin P. Numerical analysis of Biot's consolidation process by radial point interpolation method. Int J Solids Struct 2002; 39(6):1557–73.
[11] Wang JG, Liu GR, Wu YG. A point interpolation method for simulating dissipation process of consolidation. Comput Meth Appl Mech Engng 2001;190(45):5907–22.
[12] Gu YT, Liu GR. A boundary point interpolation method (BPIM) using radial function basis. In: Bathe KJ, editor. Computational fluid and solid mechanics. First MIT Conference on Computational Fluid and Solid Mechanics, USA: MIT; 2001. p. 1590–2.
[13] Rippa S. An algorithm for selecting a good value for the parameter c in radial basis function interpolation. Adv Comput Math 1999;11: 193–210.
[14] Golberg MA, Chen CS, Bowman H. Some recent results and proposals for the use of radial basis functions in the BEM. Engng Anal Bound Elem 1999;23:285–96.
[15] Golberg MA, Chen CS, Karur SR. Improved multiquadric approximation for partial differential equations. Engng Anal Bound Elem 1996;18:9–17.
[16] Kansa EJ. A scattered data approximation scheme with application to computational fluid-dynamics—I and II. Comput Math Appl 1990;19: 127–61.
[17] Fasshauer GE. Solving partial differential equations by collocation with radial basis functions. In: Mehaute AL, Rabut C, Schumaker LL, editors. Surface fitting and multiresolution methods. ; 1997. p. 131–8.
[18] Wendland H. Meshless Galerkin method using radial basis functions. Math Comput 1999;68(228):1521–31.
[19] Coleman CJ. On the use of radial basis functions in the solution of elliptic boundary value problems. Comput Mech 1996;17:418–22.
[20] Zhang X, Song KZ, Liu MW, Lu X. Meshless methods based on collocation with radial basis functions. Comput Mech 2000;26(4): 333–43.
[21] Powell MJD. The theory of radial basis function approximation in 1990. In: Light FW, editor. Adv Numer Anal. ; 1992. p. 105–203.
[22] Hardy RL. Theory and applications of the multiquadrics—Biharmonic method (20 years of discovery 1968–1988). Comput Math Appl 1990;19:163–208.
[23] Timoshenko SP, Goodier JN. Theory of elasticity. New York: McGraw-Hill; 1970.